



# Thermal boundary layers in turbulent Rayleigh-Bénard convection with rough and smooth plates: A one-to-one comparison

Ronald du Puits \*

*Institute of Thermodynamics and Fluid Mechanics, Technische Universitaet Ilmenau,  
98684 Ilmenau, Germany*

 (Received 20 November 2023; accepted 24 January 2024; published 13 February 2024)

Turbulent convection at rough surfaces covers a large variety of heat transfer processes in nature and engineering. However, in particular the transport of heat near the rough surface is still not well understood. We present measurements of the near-wall temperature field in turbulent Rayleigh-Bénard convection with rough walls, and for reference also with smooth walls. The measurements have been undertaken in a large-scale convection experiment, the “Barrel of Ilmenau.” Our experiments covered Rayleigh numbers in a domain  $5.4 \times 10^9 < Ra < 9.6 \times 10^{11}$  and two different aspect ratios  $\Gamma = 1.1$  and  $2.9$ . The working medium was air with a Prandtl number  $Pr = 0.7$ . Using very tiny micro-thermistors of  $150 \mu\text{m}$  diameter and  $350 \mu\text{m}$  length, we conducted highly resolved measurements of the temperature field near the heated bottom plate. Our measurements show that, as was already observed in high Prandtl number fluids, the ratio between the thickness of the thermal boundary layer  $\delta_{\text{th}} = H/(2Nu)$  and the roughness height  $h$  plays a crucial role for the near-wall temperature field, and thus for the convective heat transport. If  $\delta_{\text{th}}/h > 1$ , the temperature field at the rough surface does not differ from that at the smooth one. If this ratio falls below  $\delta_{\text{th}}/h = 1$ , both the mean temperature field and the temperature fluctuations start to change and to differ from that at the smooth surface. These variations are virtually independent of the Rayleigh number in the parameter domain we investigated.

DOI: [10.1103/PhysRevFluids.9.023501](https://doi.org/10.1103/PhysRevFluids.9.023501)

## I. INTRODUCTION

Thermal convection is a thermodynamical process that describes the transport of heat from a solid body or a surface to a surrounding fluid. To study this process in laboratory experiments or modeling it using numerical simulations, the surface is frequently considered as smooth [1–9]. Real processes in nature or in technical applications quite often do not meet this assumption and are, therefore, (still) hard to predict. Typical examples from nature are the heat exchange between the Earth’s ground and the atmosphere above hilly or urbanized areas or at the bottom of the oceans. In technical applications, such as, e.g., in heat exchangers or the cooling of electronic components, the efficiency of heat transfer is routinely increased by roughness elements.

Rayleigh-Bénard (RB) convection, the heat transport across a fluid layer heated from below and cooled from above, has been established as one of the preferential setups to study thermal convection in detail (for reviews, see, e.g., [10–13]). Considering a thickness  $H$  of the fluid layer and a vertical temperature drop  $\Delta T$  across it, the Rayleigh number

$$Ra = \frac{\beta g \Delta T H^3}{\nu \kappa} \quad (1)$$

\*ronald.dupuits@tu-ilmenau.de

describes the thermal forcing of the process. The other variables in this definition are  $\beta$ , thermal expansion coefficient;  $g$ , gravitational acceleration;  $\nu$ , kinematic viscosity; and  $\kappa$ , thermal diffusivity. The ratio of the latter two quantities also defines the Prandtl number:

$$\text{Pr} = \frac{\nu}{\kappa}, \quad (2)$$

the quantity that describes the properties of the fluid. If the fluid layer is laterally confined by a sidewall/sidewalls, the ratio between the lateral extent  $D$  and the thickness  $H$  of the layer

$$\Gamma = \frac{D}{H} \quad (3)$$

extends the set of input parameters. This quantity is commonly referred to as the aspect ratio. The output of the RB system, the typical fluid flow velocity within, and the heat transport across the fluid layer are usually described by the Reynolds and the Nusselt numbers:

$$\text{Re} = \frac{UH}{\nu}, \quad (4)$$

$$\text{Nu} = \frac{\dot{q}_c}{\dot{q}_d}. \quad (5)$$

Here,  $U$  denotes the typical velocity, and  $\dot{q}_c$  and  $\dot{q}_d$  stand for the convective and the diffusive heat flux, respectively. The relations between the Rayleigh number  $\text{Ra}$  and both the Reynolds and Nusselt numbers, respectively, are almost always expressed as power laws:

$$\text{Re} = C_1 \text{Ra}^\alpha, \quad (6)$$

$$\text{Nu} = C_2 \text{Ra}^\gamma. \quad (7)$$

Roughness at the horizontal plates was introduced in RB experiments in the late 1990s by Shen *et al.* [14], primarily simply to increase the heat transfer. Later on, roughness also served to disturb the boundary layers (the thin fluid layers adjacent to the horizontal walls) and to achieve the so-called ultimate regime of convection [15]. In this context, Roche *et al.* reported experiments in an RB cell whose complete interior is covered by V-shaped grooves [16]. The authors used helium at very low temperature, enabling them to cover an extremely broad domain of 11 decades in Rayleigh in their experiments. They demonstrated that, as long as the thermal boundary layer  $\delta_{\text{th}} = H/(2\text{Nu})$  is thicker than the depth of the grooves  $h$ , the heat flux across the fluid layer is not affected by the roughness. If  $\delta_{\text{th}}$  falls below  $h$ , the thermal boundary layer thickness is fixed by  $h$  and the exponent  $\gamma$  in Eq. (7) changes to the asymptotic value  $\gamma = 0.5$ . Later on, various kinds of roughness of different shape, height, and separation have been used. This comprises pyramids [17–19], spheres [20], cuboids [21–24], and ratched-like elements [25]. In almost all these experiments, water or another liquid with  $\text{Pr} \geq 2.5$  have been used. The only RB experiment with rough surfaces and air as working fluid ( $\text{Pr} = 0.7$ ) was to our knowledge the Ilmenau Barrel [22]. From all experiments mentioned above, the Lyon experiment, a cylindrical RB cell that was 0.5 m in diameter and 1.0 m in height, achieved the absolute highest Rayleigh number ( $\text{Ra} \approx 10^{15}$ ) so far [21]. In all other experiments, the Rayleigh number does not exceed  $\text{Ra} \approx 5 \times 10^{10}$ . There are also a number of direct numerical simulations (DNSs) that have modeled turbulent RB convection with rough horizontal surfaces. Due to the numerical effort, which is necessary to resolve the surface structure and the fluid flow around, the majority of those simulations only modeled two-dimensional (2D) geometries [26–29]. The simulations also covered various working fluids and roughness types. Very recently, a few papers were published that already report 3D DNSs [30–33]. Along with the structure of the pattern, the uniformness/nonuniformness of the roughness height can also affect the relation  $\text{Nu} = C_2 \text{Ra}^\gamma$ . Roughness elements of uniform height transiently increase the exponent  $\gamma$  if the  $\text{Ra}$  number rises. But, at a certain point,  $\gamma$  falls back to the value at a smooth surface [34]. This can be protruded applying roughness elements of different height [35]. Ciliberto *et al.* and Zhu *et al.*

demonstrated that the increase of the exponent  $\gamma$  can be sustained up to much higher Ra numbers when the height of the roughness elements is distributed according to a power law [20,36].

In all the above-mentioned papers, the authors emphasized the key role of the boundary layers to set the global heat transport Nu across the fluid layer. According to this previous work, one can classify RB convection with rough surfaces basically into three regimes/classes, which essentially depend on the ratio between the thickness of the thermal boundary layer  $\delta_{th} = H/(2Nu)$  and the height  $h$  and the distance  $d$  of the roughness elements:

Class I:  $\delta_{th} \gg h$ : The surface of the horizontal plates can be considered as hydraulically smooth,  $Nu_r = Nu_s$  ( $Nu_r$  and  $Nu_s$  are the dimensionless heat fluxes in a cell with either rough or smooth plates).

Class II:  $\delta_{th} \leq (h)$ : The boundary layer thickness is equal to or slightly smaller than the roughness height. It is significantly disturbed by the roughness elements, and authors frequently observed that the emission of plumes intensifies. With respect to RB convection with smooth plates, at least the prefactor  $C_2$  in Eq. (7) increases. However, it is still under discussion whether the exponent  $\gamma$  remains constant, grows at least transiently, or attains a higher value if the Rayleigh number increases. One hypothesis says that this may depend on the uniformity or nonuniformity of the height of the roughness elements [35].

Class III:  $\delta_{th} \ll h$  and/or  $\delta_{th} \ll d$ : The boundary layer thickness is much smaller than the roughness height (as many as one order of magnitude) and it follows essentially the shape of the obstacles. The exponent  $\gamma$  in Eq. (7) transiently increases with rising Ra, but with even higher Ra it falls back to the “smooth” value [34]. Employing multiscale roughness, the Ra number range of the increased  $\gamma$  can be enhanced.

In the work presented here, we focus on RB convection with uniform roughness height. Unlike in the experiments in the past, we used air as the working fluid. Its Prandtl number amounts to  $Pr = 0.7$ , significantly smaller than that of water or other fluids used in the past. This has consequences for the ratio between the thicknesses of the velocity and the thermal boundary layers  $\delta_v/\delta_{th}$  ( $>3$  for water,  $\approx 1$  for air), and therefore it generally changes the momentum and heat transport in between and above the roughness elements. We run highly resolved measurements of the near-wall temperature field as well at the rough as, for reference, at the smooth surface. This enables us to directly compare both scenarios and to precisely document the variations between both cases. Moreover, we are able to extend the Rayleigh number towards  $Ra = 10^{12}$ . This is about two orders of magnitude higher than equivalent 3D DNSs actually have achieved, and about one order of magnitude higher than in almost all previous experiments (except the one by Rusaouën *et al.* [37]). The main aim of our work is to evaluate the findings from the water experiments and the DNSs and how they can be transferred to a low Prandtl number fluid like air. As a second goal, we wish to provide a detailed comparison of the near-wall temperature field in turbulent RB convection once measured at a rough surface, the other once at a smooth one. This might be of interest in particular for those people who model thermal convection, e.g., with large eddy simulations, and who require wall functions.

Our paper is structured as follows. In the next section, we present the experimental setup and the metrology we have used for our work. In Sec. III, we describe the process of measuring the near-wall temperature field and the settings of the parameter we adjusted. In Sec. IV, we discuss the mean temperature field as well as the fluctuating one. Section V contains a summary of the work presented in this paper.

## II. EXPERIMENTAL SETUP AND MEASUREMENT TECHNIQUE

We have run our experiments in a large-scale convection facility that is called the “Barrel of Ilmenau” [BOI; see Fig. 1(a)]. It is an upright cylindrical tank with an inner diameter of 7.1 m and a total height of 8.0 m. It is filled with dry air ( $Pr = 0.7$ ). The tank is equipped with a fixed heating plate at the bottom. The free hanging cooling plate above can be moved up and down setting a thickness of the fluid layer between  $H = 0.2$  and 6.3 m. If one applies a temperature difference between the two plates, heat is released at the top surface of the heating plate, transported

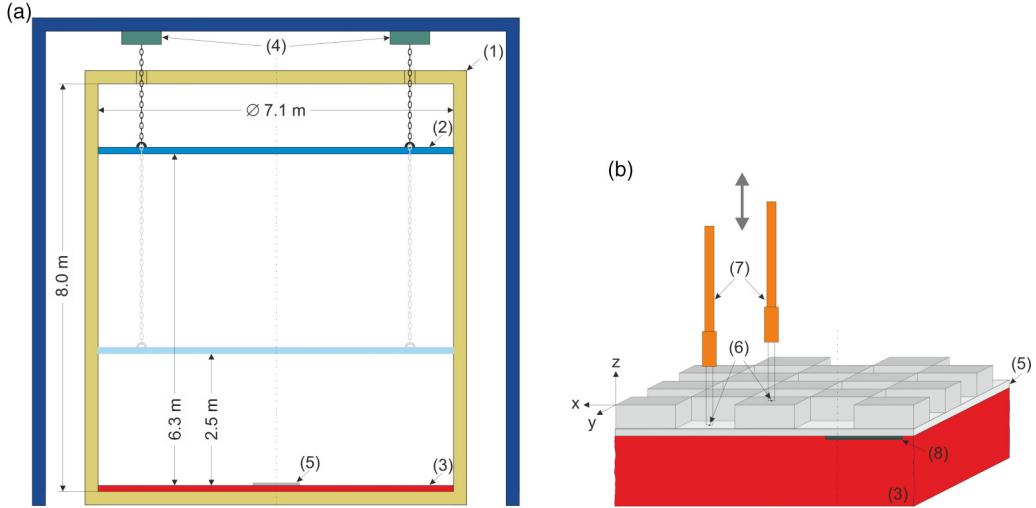


FIG. 1. (a) Principal setup of the large-scale convection facility “Barrel of Ilmenau” consisting of (1) the adiabatic container, (2) the cooling plate, (3) the heating plate, (4) the cranes, and (5) the aluminum disk with the cuboid roughness elements. The drawing shows two configurations of the distance between both plates: Configuration I:  $H = 6.3$  m and  $\Gamma = 1.1$ ; Configuration II:  $H = 2.5$  m and  $\Gamma = 2.8$ . (b) Detailed sketch of a fraction of the rough surface with (6) the temperature sensors, (7) their holders, and (8) the heat flux sensor. The sketch shows the elements in the correct proportion except the temperature sensors, which are upscaled by a factor of 2 for better visibility.

by turbulent convection across the air, and absorbed at the lower surface of the cooling plate. The surface temperature of both plates is very uniform, and the deviation at any point at the surface is typically less than  $\pm 1.5\%$  of the total temperature drop between the plates. The global mean temperature of both plates typically varies not more than  $\pm 0.02$  K over the 48 h period of a profile measurement. The sidewall is insulated to the environment by two consecutive 16 and 12 cm layers of polyurethane foam. To further reduce the heat loss, heating elements are placed between the two insulation layers. They are kept at a temperature equal to that of the air inside the tank. We have checked the heat loss throughout the sidewall and found it to be low as 0.5% of the total convective heat flux in the test section [38].

We placed 336 cuboid roughness elements of 30 mm by 30 mm cross section and 12 mm height at the surface of the heating plate. They are made of aluminum and form a chessboard-like pattern with a period of  $2d = 60$  mm [see Fig. 1(b)]. We wish to point out here that, unlike in other setups discussed in Sec. I [21,22,39], our roughness pattern does not include grooves between the cuboids. This makes the pattern invariant with respect to the orientation of the turbulent wind. The cuboids are mounted at a circular aluminum disk, 950 mm in diameter and 3 mm thick, using adhesive pads with high thermal conductivity. This “rough” disk was placed at the center of the heating plate adding a 0.15-mm-thick foil of silicon rubber in the gap between the surface of the plate and the disk. The foil significantly improves the thermal contact and ensures that the temperature drop between the plate and the disk remains as small as possible. For the measurements at the smooth surface, we removed the disk temporarily. To evaluate the typical temperature drop from the heating plate to the disk and further to the top of the cuboids, we have done measurements of the temperature at the top surface of the cuboids using an infrared camera. The measurements have been undertaken at two different heights  $H$  and two temperature differences  $\Delta T$ . The results are listed in Table I. The deviation of the temperature at the top of the obstacles amounts to less than 1.4% of the total temperature drop  $\Delta T$  across the fluid layer, and it should not significantly affect the temperature field near the rough surface.

TABLE I. Temperature  $T_{\text{top}}$  at the top of the roughness elements at various distances  $H$  between the heating and the cooling plates.  $T_{\text{hp}}$  and  $T_{\text{cp}}$  denote the temperature of both plates. The last column indicates the relative deviation of  $T_{\text{top}}$  with respect to the total temperature difference  $\Delta T$ , which does not exceed 1.4% in all configurations.

$H$ (m)	$T_{\text{hp}}$ ( $^{\circ}\text{C}$ )	$T_{\text{cp}}$ ( $^{\circ}\text{C}$ )	$T_{\text{top}}$ ( $^{\circ}\text{C}$ )	$ \frac{(T_{\text{top}} - T_{\text{hp}})}{(T_{\text{hp}} - T_{\text{cp}})} $
1.45	24.97	20.00	24.92	0.010
1.45	59.78	20.00	59.20	0.014
5.40	24.86	20.00	24.98	0.025 <sup>a</sup>
5.40	49.94	10.00	49.59	0.009

<sup>a</sup>This positive deviation of 0.12 K is probably caused by the measurement uncertainty of the infrared camera.

Another issue we wish to discuss here is the fact that we did not fully cover the heating and the cooling plates with cuboids. This is simply a matter of effort, since it would require about 38 000 cuboids to make the entire surface of both plates (80 m<sup>2</sup>) rough. In this context, we recall the work of Tisserand *et al.* [21], who found that the fully turbulent flow in the bulk (i.e., the flow region far from the plates and the sidewall, where the temperature of the fluid is uniform) is almost not affected by the roughness. Nevertheless, we took care that the roughness covers a sufficiently large radius around the measurement position. As mentioned above, the radius of the rough disk amounts to 475 mm. Depending on the Rayleigh number  $Ra$  and the distance between the heating and the cooling plates  $H$ , it corresponds to 20–100 times the thickness of the boundary layer.

We used very small thermistors to measure the temperature field near the rough surface. They have an ellipsoidal shape with a typical diameter of 150  $\mu\text{m}$  and a typical length of 350  $\mu\text{m}$ . They are connected via 18  $\mu\text{m}$  wires to 0.3 mm needles, which are part of the holder [see Fig. 1(b)]. The holder with the thermistors could be moved in steps of 10  $\mu\text{m}$  up and down. We used two of them to simultaneously measure the temperature at the top of one cuboid and in one valley in between the cuboids. The thermistors were connected to an in-house two-channel dc bridge with an internal amplifier. The bridge operates with a very low measurement current of 5  $\mu\text{A}$ . This is sufficiently small to limit the self-heating of the sensors to a value below 10 mK. A PC-based data acquisition system with a resolution of 18 bits recorded the output signals of the bridge with a rate of 50 samples/s. Before we used the thermistors in the BOI, we calibrated them against a certified PT-100 in a calibration chamber. The remaining uncertainty of  $\pm 20$  mK was further reduced by an *in situ* calibration in the measurement chamber. For the latter, we used the temperature of a PT-100 sensor, which was placed in the well-mixed bulk flow as a reference value for the thermistor's bulk temperature.

A specific requirement on temperature measurements in turbulent flows is the capability of the sensor to track even the fastest temperature fluctuations in the flow. This depends not only on the properties of the sensor, but also on the characteristics of the flow around it. More precisely, this is mainly related to the size and the advection velocity of the smallest vortices in the turbulent flow. A good estimation for the required resolution in space and time is the Kolmogorov microscales  $\eta = (\nu^3/\varepsilon)^{1/4}$  and  $\tau_\eta = (\nu/\varepsilon)^{1/2}$ , with  $\nu$  and  $\varepsilon$  being the kinematic viscosity and the rate of dissipation of turbulent kinetic energy, respectively. We have listed these two quantities for all sets of  $\Gamma$  and  $Ra$  we investigated in Table II.

To resolve these scales, the sensor has to be smaller and faster than the corresponding numbers. This demand is fulfilled very well for the size of our thermistor. We have also evaluated the response time of the thermistor in a simple laboratory setup. This is shown in the left subfigure of Fig. 2. The thermistor was placed in a well-defined laminar flow, whose velocity could be set between 0.0 and 1.0 m/s. This is the typical domain of flow velocity in our convection experiment. Using a laser beam, we heated the sensor up. Having achieved a steady state, we switched the laser off, and we measured the decay time. It is quite common to quantify this curve in a single value—the

TABLE II. Kolmogorov microscales  $\eta$  and  $\tau_\eta$  for all sets of  $\Gamma$  and Ra we investigated.  $H$  stands for the vertical extent of the fluid layer.  $U = \text{Re}_{\text{GL}}H/\nu$  is the typical velocity of the flow computed with the Reynolds number  $\text{Re}_{\text{GL}}$  according to the Grossmann-Lohse theory [40].

$\Gamma$	Ra	$H$ (m)	$U$ (m/s)	$\eta$ (mm)	$\tau_\eta$ (s)
1.1	$5.8 \times 10^{10}$	6.3	0.068	3.0	0.563
1.1	$8.6 \times 10^{10}$	6.3	0.081	2.5	0.369
1.1	$1.5 \times 10^{11}$	6.3	0.104	2.0	0.252
1.1	$2.2 \times 10^{11}$	6.3	0.122	1.8	0.196
1.1	$4.3 \times 10^{11}$	6.3	0.165	1.4	0.128
1.1	$6.3 \times 10^{11}$	6.3	0.197	1.3	0.100
1.1	$8.0 \times 10^{11}$	6.3	0.219	1.2	0.082
1.1	$9.6 \times 10^{11}$	6.3	0.255	1.1	0.069
2.9	$5.4 \times 10^9$	2.5	0.061	2.7	0.442
2.9	$9.4 \times 10^9$	2.5	0.077	2.2	0.297
2.9	$1.3 \times 10^{10}$	2.5	0.091	1.9	0.228
2.9	$2.7 \times 10^{10}$	2.5	0.123	1.6	0.148
2.9	$4.0 \times 10^{10}$	2.5	0.146	1.4	0.114
2.9	$5.1 \times 10^{10}$	2.5	0.163	1.2	0.096
2.9	$5.9 \times 10^{10}$	2.5	0.187	1.2	0.081

response time  $\tau_{70}$ . The quantity is a measure of the period the sensor needs to achieve 70% of the total jump between the high and the low temperature. We follow this and plot  $\tau_{70}$  of our microthermistor in the right subfigure of Fig. 2. If one compares the values of the Kolmogorov timescales and the typical velocities in Table II with the response time, one ascertains that the sensor is not sufficiently fast for all sets of parameters. If the Rayleigh number exceeds  $\text{Ra} = 4.3 \times 10^{11}$  ( $\Gamma = 1.1$ ) and  $\text{Ra} = 2.7 \times 10^{10}$  ( $\Gamma = 2.9$ ), this requirement was not fulfilled and the measured amplitude of the temperature fluctuations might be smaller than the real fluctuations in the flow.

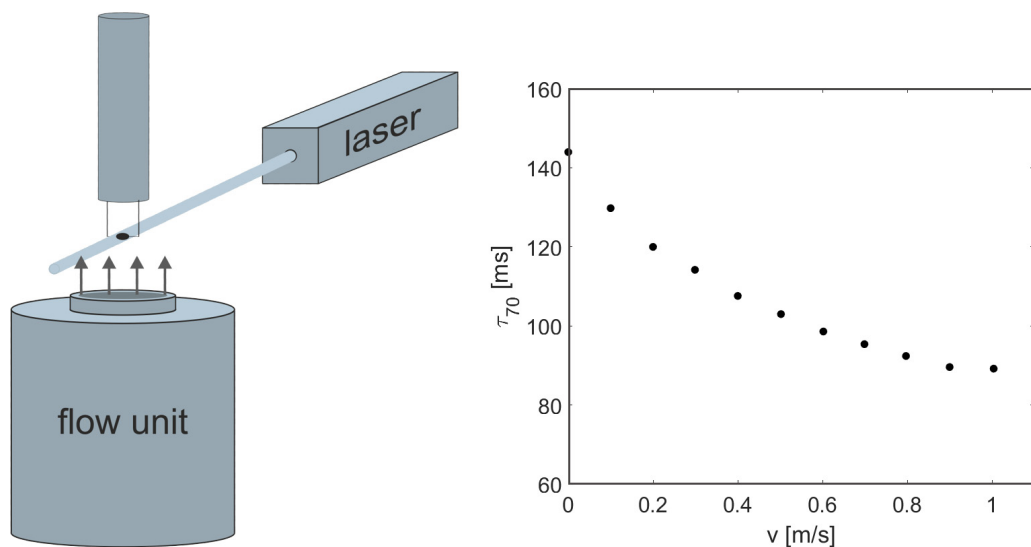


FIG. 2. Left: Laboratory setup to measure the response time of the temperature sensor under well-defined flow conditions. Right: Measured response time  $\tau_{70}$  with respect to the flow velocity.

TABLE III. Set of parameters for the temperature measurements at the rough and the smooth surface. The Nusselt number  $Nu$  results from direct measurements of the local wall heat flux at the smooth plate. We also give the boundary layer thickness  $\delta_{th} = H/(2Nu)$  as a reference with respect to the roughness height  $h$ .

$\Gamma$	Ra	$\Delta T$ (K)	$T_b$ ( $^{\circ}\text{C}$ )	$H$ (m)	Nu	$\delta_{th}$ (mm)	$\delta_{th}/H$ ( $10^{-3}$ )
1.1	$5.8 \times 10^{10}$	2.7	30.4	6.3	164.2	19.18	3.04
1.1	$8.6 \times 10^{10}$	4.0	30.5	6.3	256.8	12.26	1.95
1.1	$1.5 \times 10^{11}$	7.0	30.6	6.3	313.9	10.04	1.59
1.1	$2.2 \times 10^{11}$	10.0	30.8	6.3	361.6	8.71	1.38
1.1	$4.3 \times 10^{11}$	20.0	31.2	6.3	429.2	7.34	1.17
1.1	$6.3 \times 10^{11}$	30.0	31.6	6.3	471.5	6.68	1.06
1.1	$8.0 \times 10^{11}$	38.0	31.8	6.3	542.8	5.80	0.92
1.1	$9.6 \times 10^{11}$	55.0	45.0	6.3	559.0	5.64	0.90
2.9	$5.4 \times 10^9$	4.0	30.3	2.5	71.7	17.44	6.98
2.9	$9.4 \times 10^9$	7.0	30.5	2.5	90.4	13.82	5.53
2.9	$1.3 \times 10^{10}$	10.0	30.6	2.5	106.4	11.75	4.70
2.9	$2.7 \times 10^{10}$	20.0	31.1	2.5	127.1	9.83	3.93
2.9	$4.0 \times 10^{10}$	30.0	31.5	2.5	143.4	8.72	3.49
2.9	$5.1 \times 10^{10}$	38.0	30.5	2.5	160.6	7.78	3.11
2.9	$5.9 \times 10^{10}$	54.7	43.7	2.5	165.0	7.58	3.03

We have also embedded five heat flux sensors (PhyMeas, Type 3) into the surface of the heating plate to measure the local wall heat flux [see Fig. 1(b)]. The sensors are disks with a well-defined heat conductivity. Their diameter amounts to 33 mm, while they are only 1.5 mm thick. Thermocouples at the lower and the upper side of the disk provide a thermoelectric voltage. It is proportional to the temperature drop across the heat flux plate, and thus also to the local wall heat flux. We have assembled one sensor at the plate's center nearly below the position of the temperature sensors. The other four sensors are located at a circular ring of 850 mm diameter with a  $90^{\circ}$  angle in between them.

### III. MEASUREMENT PROCEDURE

One particular aim of the study we report here is to compare one-to-one the near-wall temperature field at a rough surface with that at a smooth one. In this sense, we have run our measurements first above the rough surface, and then, at the same Rayleigh number and the same aspect ratio, at the smooth one. The main parameters of all measurements are listed in Table III. Our experiments span two and a half decades in Rayleigh number  $5.4 \times 10^9 < Ra < 9.6 \times 10^{11}$  and cover two different aspect ratios  $\Gamma = 1.1$  and 2.9. With respect to these two aspect ratios, we denote our settings as Configurations I and II. To vary the Rayleigh number within a single aspect ratio, we changed the temperature difference  $\Delta T$ . The temperature of the heating and the cooling plates was always set symmetrically above and below a temperature of  $30.0^{\circ}\text{C}$ , except for the measurements at  $\Gamma = 1.1$ ,  $Ra = 9.6 \times 10^{11}$  and  $\Gamma = 2.9$ ,  $Ra = 5.9 \times 10^{10}$ . For those measurements, the theoretical middle amounted to  $42.5^{\circ}\text{C}$ . We have measured the near-wall temperature field in and above the valley and above the top of the cuboids simultaneously using two of the micro-thermistors. They are placed at the centers of one valley and one cuboid very close to the central axis of the experiment. They are mounted at a single traverse unit, which allows them to move up and down (cf. Fig. 1).

Before we started a measurement of a temperature profile  $\Theta(z)$ , we adjusted the position  $z = 0$  mm of each thermistor separately. We moved them towards the ground surface of the valley and the top surface of the cuboid, respectively, until the thermistor touched the surface. Then we moved them back a little bit and we defined this position as  $z = -11.9$  mm for the valley and  $z = 0.1$  mm for the top of the cuboid. This smallest measurement distance of  $z = 0.1$  mm from the



surface is the sum of the radius of the thermistor (0.075 mm) and a small gap (0.025 mm) which is necessary to prevent a potential bias of the measurement closest to the wall. After finishing this process, we waited until the experiment became stationary. Then, we started the measurement at this position and we acquired the temperature with a rate of  $50^{-1}$  over a period of 90 min. We repeated this for another 31 positions  $z$  up to  $z = 138$  mm (valley) and  $z = 150$  mm (top). Having finished the measurement at the rough surface, we removed the plate with the roughness elements and proceeded in the same way at the smooth surface. Related to this measurement regime, we wish to discuss two particularities which significantly influence the results:

(1) The temperature at the various distances  $z$  from the plate surface was measured at different periods of time. Potential long-term variations of the turbulent convection flow over the total measurement period of 48 h affect the computed mean of the temperature and the fluctuations. This leads to a scatter of the data, which can significantly exceed the error of the measurement technique.

(2) The measurements of the temperature at the same position  $z$  above the valley and the top of the cuboid were undertaken during different periods of time which are shifted by 25.5 h. Deviations of the mean of the temperature and the fluctuations measured above the valley and the top are caused by the same mechanism as mentioned under Item 1.

## IV. RESULTS

### A. The mean temperature field

We start our discussion with a comparative analysis of the profiles of the mean temperature  $T(z)$  above the rough and the smooth surfaces. To make the data comparable, we scale the measured temperature by the temperature difference between the heating plate and the well-mixed bulk  $T_{\text{hp}} - T_b$ :

$$\Theta = \frac{T(z) - T_b}{T_{\text{hp}} - T_b}. \quad (8)$$

We plot a selection of the profiles of the normalized mean temperature,

$$\bar{\Theta} = \frac{1}{N} \sum_{i=1}^N \Theta_i, \quad (9)$$

for four different parameter sets in Fig. 3. Each subplot (a)–(d) contains the profiles at the top of a cuboid, in and above the valley, and as a reference the profile measured at the smooth plate. Subplots (a) and (c) show the mean temperature profiles at the lowest and the highest Rayleigh number in Configuration I ( $\Gamma = 1.13$ ), while subplots (b) and (d) display these profiles for Configuration II ( $\Gamma = 2.86$ ). In the two upper subplots (a) and (b), the temperature difference  $\Delta T$  was set to the lowest possible value, so that the resulting thickness of the boundary layer  $\delta_{\text{th}}$  is larger than the height of the cuboids  $h$  (see Table III). Considering the plane at the top of the cuboids ( $z/H = 0$ ) as equivalent to the surface of the smooth plate, the mean temperature profiles above a cuboid and above a smooth surface collapse very well. The temperature inside the valley (for  $z/H < 0$ ) decreases more slowly with increasing distance, but right above  $z/H = 0$  it approaches the level of the other two profiles. If one now increases the temperature difference  $\Delta T$  between the heating and the cooling plates, the mean temperature profiles at the rough surface start to deviate from that at the smooth one. This is shown in subplots (c) and (d) and pertains for both configurations. The deviation appears mainly at a distance where the normalized mean temperature varies between  $0.3 > \bar{\Theta} > 0.05$ . It corresponds to distances  $4.9 < z < 54.1$  mm in Configuration I and  $5.1 < z < 44.2$  mm in Configuration II. The modification of the mean temperature field is independent of whether we have measured the temperature above a cuboid or above a valley, and it mainly concerns the flow region outside the thermal boundary layer (cf. Table III). In this region, which is frequently referred to as a mixing zone [2], the advection of thermal plumes dominates the local heat transport and the temperature field is strongly coupled to the size and the frequency of these plumes. We



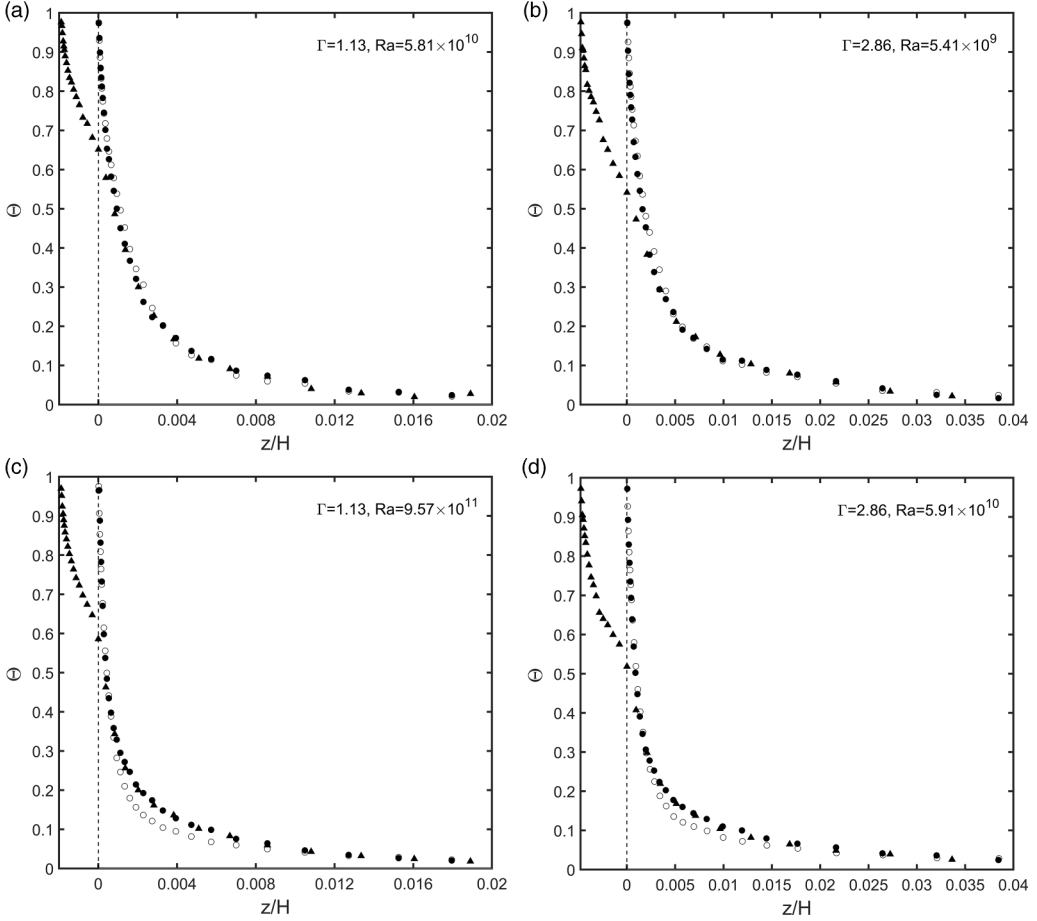


FIG. 3. Profiles of the normalized mean temperature above the center of the heating plate. Subplots (a) and (b) show profiles at the lowest temperature difference  $\Delta T$ , where the resulting boundary layer thickness  $\delta_{th}$  is larger than the roughness height  $h$ . Subplots (c) and (d) show profiles at the highest  $\Delta T$ , if  $\delta_{th}$  is smaller than  $h$  (cf. Table III). Subplots (a) and (c) represent data from Configuration I ( $\Gamma = 1.13$ ), while subplots (b) and (d) represent the equivalent data from Configuration II ( $\Gamma = 2.86$ ). Each subplot contains the mean temperature profiles at the smooth plate ( $\circ$ ), above the top of a cuboid ( $\bullet$ ), and at the valley in between the cuboids ( $\blacktriangle$ ). The dashed vertical line at  $z/H = 0$  represents the plane at the top of the cuboids.

conclude, and this is in good agreement with earlier experiments in water [17,23,24,39], that surface roughness changes the heat transport by modifying the evolution of thermal plumes. This happens, if the thickness of the thermal boundary layer falls below the height of the roughness elements. It is also important to mention that this process obviously does not depend on the Rayleigh number, since it happens at the higher Rayleigh numbers in Configuration I ( $5.8 \times 10^{10} < Ra < 9.6 \times 10^{11}$ ) as well as at the lower ones in Configuration II ( $5.4 \times 10^9 < Ra < 5.9 \times 10^{10}$ ).

In the next step, we will quantitatively analyze the modification of the mean temperature profile by the surface roughness for all Rayleigh numbers we investigated. To this aim, we plot the difference between  $\bar{\Theta}_{top}(z/H)$  at the top of the cuboids and the reference profile  $\bar{\Theta}_{smooth}(z/H)$  at the smooth surface in Fig. 4. Initially, we will focus our discussion on the left subplot, which shows  $\bar{\Theta}_{top}(z/H) - \bar{\Theta}_{smooth}(z/H)$  for Configuration I. The curves are staggered in such a way that the deviation at the lowest Rayleigh number  $Ra = 5.8 \times 10^{10}$  ( $\delta_{th} = 19.18$  mm) is shown on top. Very close to the surface, there is a thin fluid layer, in which the mean temperature at the rough surface

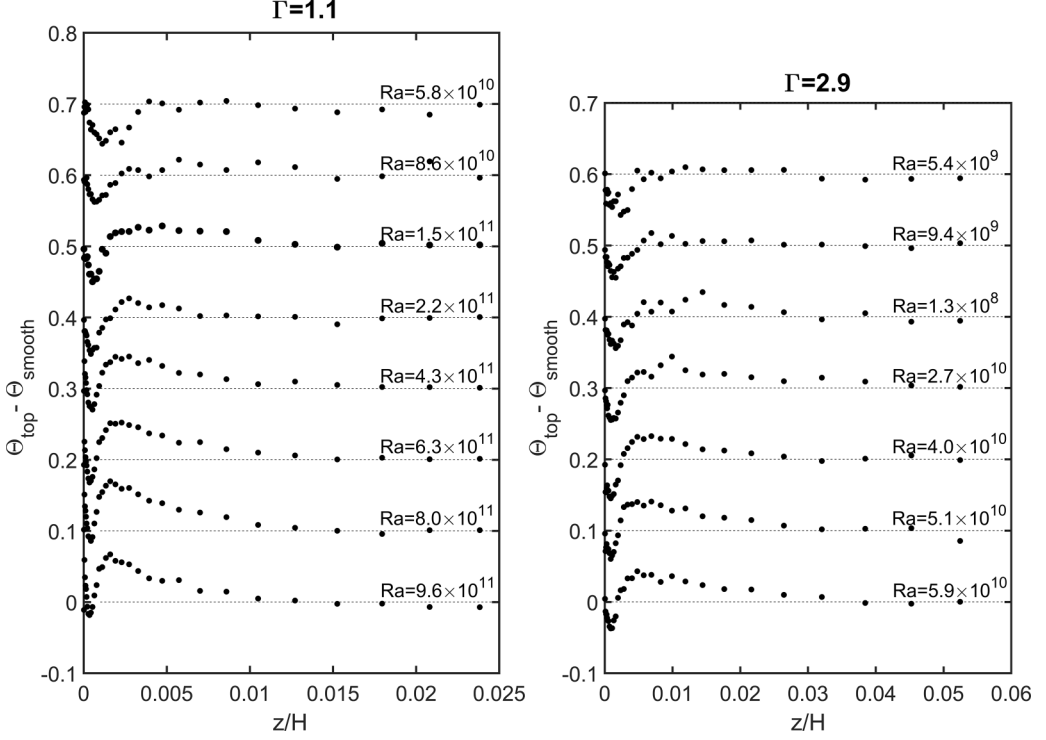


FIG. 4. Deviation of the mean temperature profiles measured above the top of the cuboids  $\bar{\Theta}_{\text{top}}(z/H)$  from the profiles  $\bar{\Theta}_{\text{smooth}}(z/H)$  measured at the smooth surface. The left plot shows this for the higher range of  $Ra$  in Configuration I ( $\Gamma = 1.1$ ), while the right plot shows this for the lower range in Configuration II ( $\Gamma = 2.9$ ). The plots are shifted by  $+0.1$  with decreasing Rayleigh number.

decreases faster than that at the smooth one. We explain this with a better mixing of the fluid due to the alternating cuboid-valley structure. Going down with the curves, the effect becomes smaller and smaller and almost vanishes at the highest Rayleigh number  $Ra = 9.6 \times 10^{11}$ . However, it is more interesting to focus our attention on the flow region beyond this very thin fluid layer. We see a first significant positive deviation  $\bar{\Theta}_{\text{top}}(z/H) - \bar{\Theta}_{\text{smooth}}(z/H)$  if the Rayleigh number achieves  $Ra = 1.5 \times 10^{11}$ . This is the Rayleigh number at which the boundary layer thickness initially falls below the height of the roughness elements ( $\delta_{\text{th}} = 10.04$  mm). Increasing the Rayleigh number again, the positive deviation becomes larger, and at  $Ra = 9.6 \times 10^{11}$ , the deviation  $\bar{\Theta}_{\text{top}} - \bar{\Theta}_{\text{smooth}}$  achieves a maximum of  $+0.07$  at  $z/H = 0.0016$ . If we move now to the right subplot of Fig. 4, we can see the same picture. Below  $Ra = 1.3 \times 10^{10}$ , there is just a little negative deviation between the profiles. But beyond this Rayleigh number ( $\delta_{\text{th}}$  falls below the roughness height  $h$ ), the mean temperature at the rough surface is again higher than at the smooth one. This is remarkable since the Rayleigh number is one decade lower than the transitional one in the left subplot. Insofar, it would be interesting to widen the Rayleigh number domain towards even higher (or lower) Rayleigh numbers. Unfortunately, we were not able to do this, since our experimental setup is limited in  $Ra$  to the values reported here.

We finish our analysis of the mean temperature field by checking a hypothesis that has been proposed by Rusaouën *et al.* quite recently [37]. The authors of this work investigated RB convection with a similar roughness structure of cuboids and valleys and water with  $2.9 < Pr < 5.5$  as working fluid. They observed a decrease of the thermal impedance of the boundary layer if the Rayleigh number becomes sufficiently large. The authors explained this effect by a turbulent destabilization

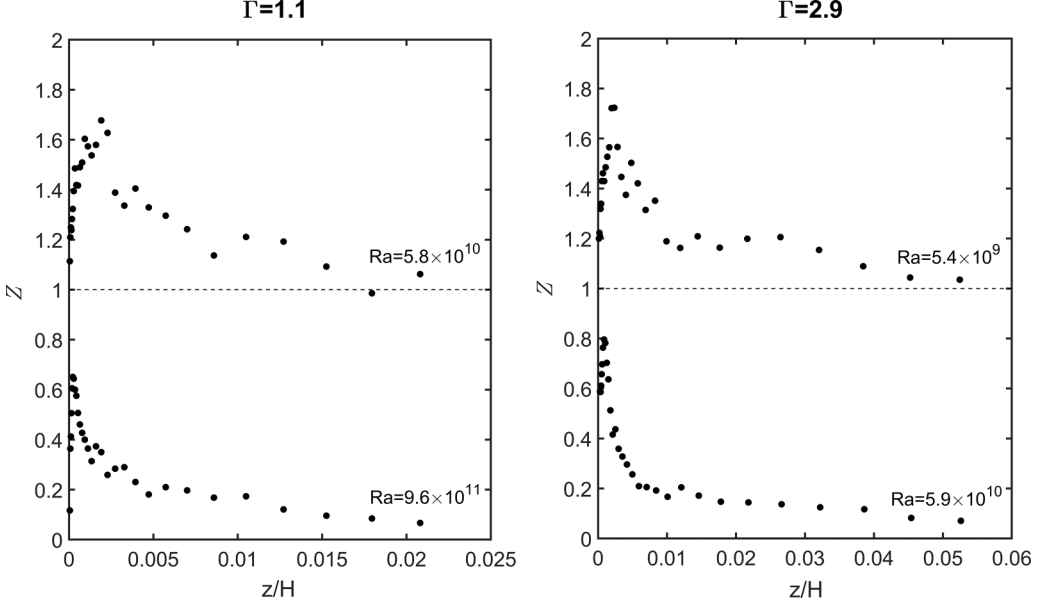


FIG. 5. Diagnostic function  $Z = d\bar{\Theta}_{\text{top}}/d[\log(z/H)]$  of the mean temperature profiles measured above the top of the cuboids. A logarithmic trend in one of the mean temperature profiles would be indicated by a plateau  $Z = \text{const}$ . The left plot shows this for the higher range of  $Ra$  in Configuration I ( $\Gamma = 1.1$ ), while the right plot shows this for the lower range in Configuration II ( $\Gamma = 2.9$ ). The diagnostic functions  $Z$  for  $Ra = 5.8 \times 10^{10}$  and  $5.4 \times 10^9$  are shifted by +1.

of the boundary layer above the top of the cuboids. Such a transition would be indicated by a logarithmic trend of the mean temperature profile  $\bar{\Theta}(z/H)$  [41]. To evaluate such a trend, we have computed the logarithmic diagnostic function  $Z$  of the mean temperature profiles for all measurements in Configurations I and II:

$$Z = \frac{d\bar{\Theta}_{\text{top}}}{d[\log(z/H)]}. \quad (10)$$

We plot it for the lowest and the highest Rayleigh numbers of both configurations in Fig. 5. In the case in which  $\bar{\Theta}_{\text{top}} \sim \log(z/H)$ , the diagnostic function would exhibit a plateau with  $Z = \text{const}$ . In fact, none of the plotted diagnostic functions shows such a plateau, and that indicates a transition towards turbulence. This is true for the measurements where the boundary layer is thicker than the roughness height ( $Ra = 5.4 \times 10^9$ ,  $Ra = 5.8 \times 10^{10}$ ) as well as for those measurements where the inverse is the case ( $Ra = 5.9 \times 10^{10}$ ,  $Ra = 9.6 \times 10^{11}$ ). On the other hand, particle image velocimetry (PIV) measurements in a very similar configuration with cuboid roughness elements undertaken by Liot *et al.* have shown that the boundary layer above the top of the cuboids indeed may become turbulent even though the Rayleigh number did not exceed  $Ra = 4 \times 10^{10}$  [22]. We will stop this discussion here and will return to this subject at the end of Sec. IV B.

### B. The fluctuating temperature field

In this section, we will discuss the fluctuating temperature field  $\Theta'(z)$ . In addition, we normalize the fluctuations by the temperature difference  $T_{\text{hp}} - T_b$  yielding

$$\Theta' = \sqrt{\frac{1}{N} \sum_{i=1}^N (\Theta_i - \bar{\Theta})^2}. \quad (11)$$

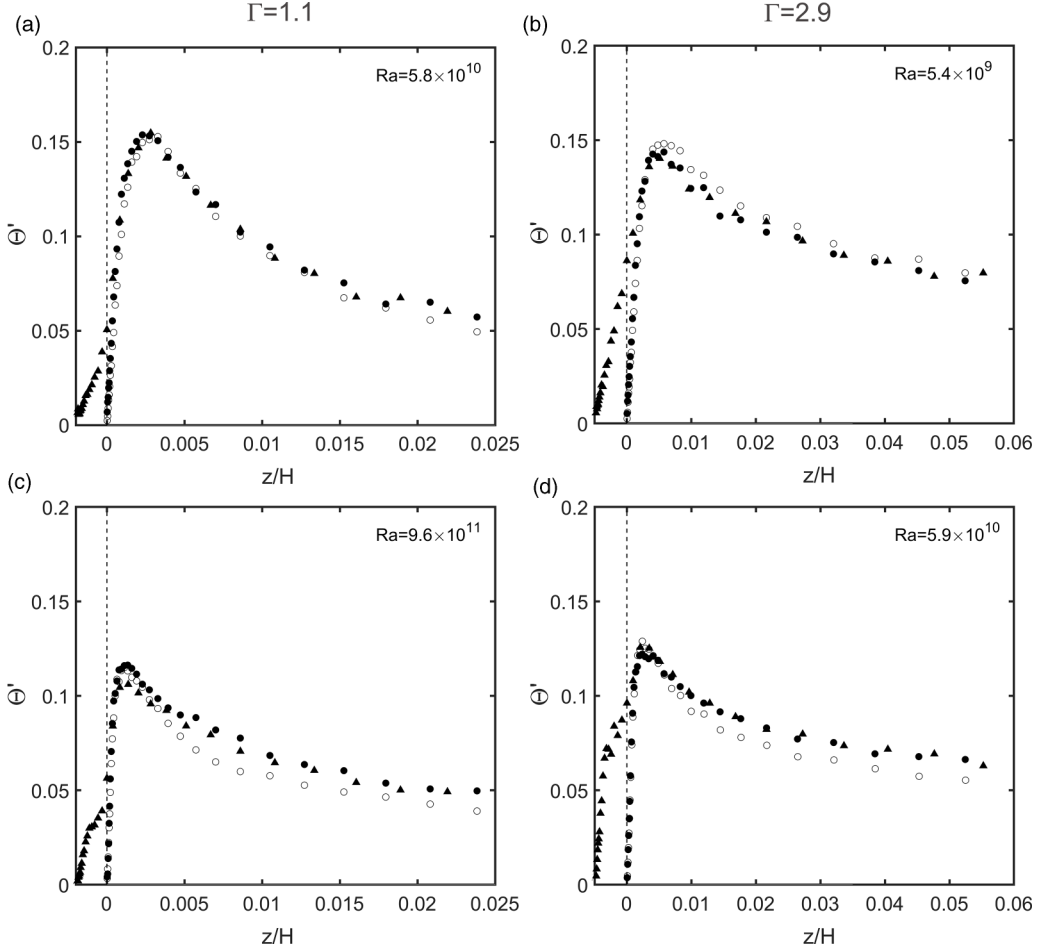


FIG. 6. Profiles of the normalized temperature fluctuations  $\Theta'(z/H)$  above the center of the heating plate. The subplots (a) and (b) show profiles if the boundary layer thickness  $\delta_{th}$  is larger than the roughness height  $h$ , while the subplots (c) and (d) show profiles if  $\delta_{th}$  falls below  $h$  (cf. Table III). The subplots (a) and (c) represent data for the lowest and the highest Rayleigh number in Configuration I ( $\Gamma = 1.13$ ), while subplots (b) and (d) represent the equivalent data from Configuration II ( $\Gamma = 2.86$ ). Each subplot contains the profiles of the temperature fluctuations above the top of the cuboids ( $\bullet$ ), at the valley in between them ( $\blacktriangle$ ), and, as a reference, at the smooth plate ( $\circ$ ). The dashed vertical line at  $z/H = 0$  represents the plane at the top of the cuboids.

Before we start our discussion, we wish to remind the reader of the limitation of the sensor to follow very fast temperature fluctuations (cf. Sec. II). This limitation may affect the measurements at  $\Gamma = 1.1$  and  $Ra > 4.3 \times 10^{11}$  and at  $\Gamma = 2.9$  and  $Ra > 2.7 \times 10^{10}$ . As a consequence, the measured temperature fluctuations  $\Theta'$  might be smaller than the real ones. However, since we are mainly focusing our discussion on the differences of the fluctuating temperature above a rough and a smooth surface, these measurement errors do not play any role.

We start our discussion plotting four selected profiles of the normalized temperature fluctuations  $\Theta'(z/H)$  in Fig. 6. The profiles cover the lowest and the highest Rayleigh number for each of Configurations I and II. In analogy to Fig. 3, the two upper subplots (a) and (b) show the profiles when the thickness of the boundary layer  $\delta_{th}$  exceeds the height of the cuboids  $h$ , while the lower two subplots (c) and (d) show the profiles for the reverse case. Again, we have added the equivalent profiles above a smooth surface for reference. Initially, we focus on the fluctuating field for  $z/H > 0$ .

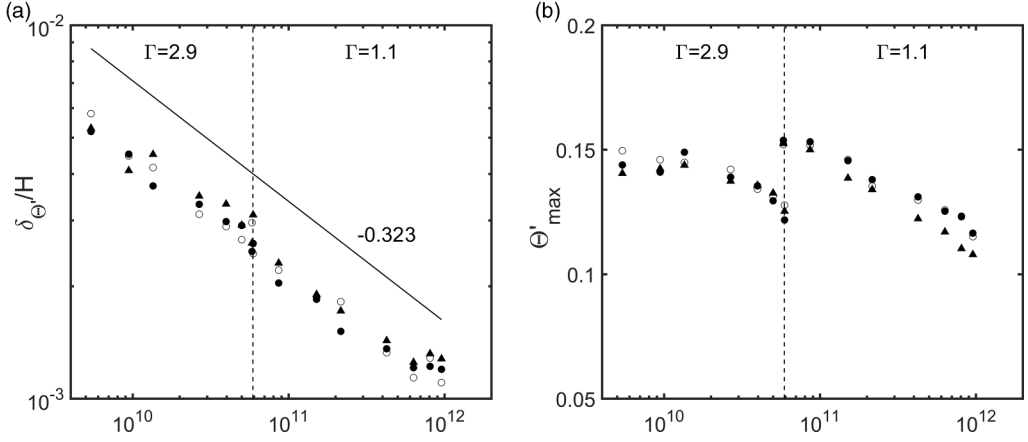


FIG. 7. Position of the maximum of the normalized temperature fluctuations  $\delta_{\Theta'}/H$  (a) and the maximum  $\Theta'_{\max}$  itself (b) plotted vs Rayleigh number. The  $\blacktriangle$  symbols and the  $\bullet$  symbols represent the data above the valleys and the top of the cuboids, respectively, while the ( $\circ$ ) symbols stand for the data at the smooth surface. The line in subplot (a) indicates a power-law fit  $\delta_{\Theta'}/H \sim Ra^\gamma$  with  $\gamma = -0.323$ .

In all four subplots, the profiles  $\Theta'(z/H)$  collapse quite well with the equivalent profiles above a smooth surface independent of whether they are measured above a cuboid or a valley. The temperature fluctuations above the rough surface tend to decrease a bit more slowly for the highest Rayleigh number. All profiles  $\Theta'(z/H)$  exhibit a maximum  $\Theta'_{\max}$  which moves towards the plate surface if the Rayleigh number increases. We define the position of this maximum as  $\delta_{\Theta'}$  and plot this quantity versus all measured Rayleigh numbers in Fig. 7(a). Despite the scatter of the data points, which is mainly caused by the fact that the experiments with the rough and the smooth surface were undertaken at different times, the  $\delta_{\Theta'}$  at the rough and the smooth data set collapse fairly well. About the entire domain of Ra, a power law with an exponent  $\xi = -0.323$  seems to be the best fit for  $\delta_{\Theta'} \sim Ra^\xi$ . In Fig. 7(b), we plot the maximum  $\Theta'_{\max}$  itself. In addition, the maximum of the temperature fluctuations at the rough surface does not differ significantly from that at the smooth one. There is also a fair agreement between  $\delta_{\Theta'}$  and the boundary layer thickness based on the Nusselt number  $\delta_{th}$ . Within each of Configurations I and II, the maximum of the normalized fluctuations starts with  $\Theta'_{\max} \approx 0.15$  at the lowest Rayleigh number/temperature difference. It decreases with increasing Rayleigh number/temperature difference and ends up at  $\Theta'_{\max} \approx 0.12$ . We assume that this is an artefact of the thermal inertia of the sensor (see the discussion in Sec. II). However, based on our data, we cannot rule out that the decrease of  $\Theta'_{\max}$  is real.

In the next step, we will check an observation that has been made as well in recent DNSs by Belkadi *et al.* [32] as in experiments by Liot *et al.* [22]. Both authors reported that the fluid is at rest and trapped in the valleys if the thickness of the thermal boundary layer  $\delta_{th}$  exceeds the height  $h$  of the cuboids. Its stratification starts to become unstable if  $\delta_{th}$  achieves the order of  $h$ . If the Rayleigh number is further increased, the fluid in the valleys starts to exchange with the fluid above the obstacles, which significantly enhances the heat transfer from the surface. This process should be visible as well in the profiles of the normalized temperature fluctuations  $\Theta'$ . And indeed, comparing Figs. 6(a) and 6(c) and Figs. 6(b) and 6(d), respectively, one can see a clear difference. To make these differences more clear, we again plot a few selected profiles  $\Theta'(z/H)$  for  $z/H < 0$  in Fig. 8. The profiles are those at the two lowest Rayleigh numbers (open symbols) and those at the two highest Rayleigh numbers (full symbols) of each configuration. The first thing we can see immediately is that the temperature fluctuations in the valleys are not zero even at the lowest Rayleigh number we could set in both configurations (see the  $\triangle$  symbols). This indicates that the fluid is not fully at rest in the valleys, even if  $\delta_{th} > h$ . Nevertheless, if one

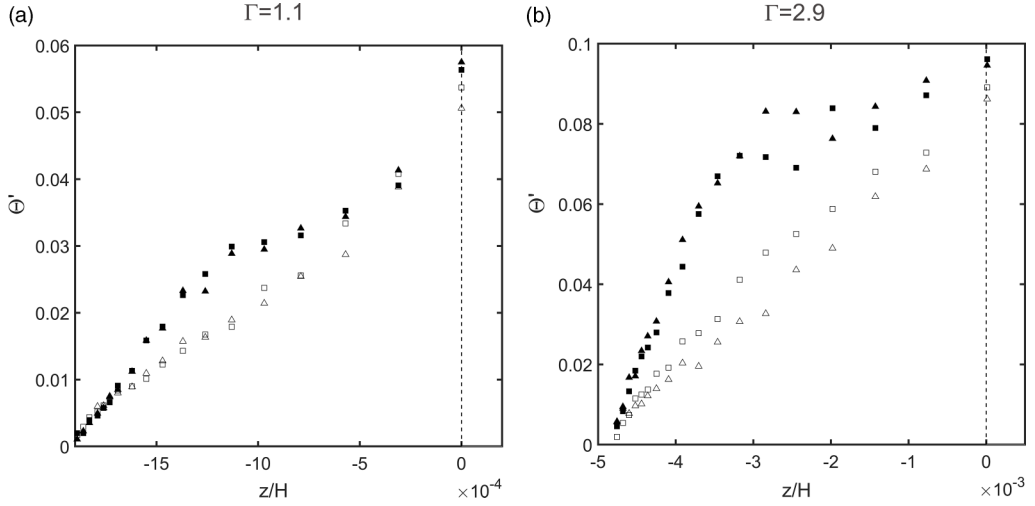


FIG. 8. Profiles of the normalized temperature fluctuations  $\Theta'(z/H)$  in the valley for Configuration I ( $\Gamma = 1.13$ ) (a) and Configuration II ( $\Gamma = 2.86$ ) (b). (a) Data at  $Ra = 5.8 \times 10^{10}$  ( $\Delta$ ) and  $Ra = 8.6 \times 10^{10}$  ( $\square$ ), where  $\delta_{th} > h$  as well as the data at  $Ra = 8.0 \times 10^{11}$  ( $\blacktriangle$ ) and  $Ra = 9.6 \times 10^{11}$  ( $\blacksquare$ ), where  $\delta_{th} < h$ . (b) Data at  $Ra = 5.4 \times 10^9$  ( $\Delta$ ) and  $Ra = 9.4 \times 10^9$  ( $\square$ ), where  $\delta_{th} > h$  as well as the data at  $Ra = 5.1 \times 10^{10}$  ( $\blacktriangle$ ) and  $Ra = 5.9 \times 10^{10}$  ( $\blacksquare$ ), where  $\delta_{th} < h$ .

increases the Rayleigh number and  $\delta_{th}$  falls below  $h$ , the temperature fluctuations become larger. This effect is more pronounced in Configuration II ( $\Gamma = 2.86$ ), where the Rayleigh number varies between  $5.4 \times 10^9 < Ra < 5.9 \times 10^{10}$ , than in Configuration I ( $\Gamma = 1.13$ ), where it varies between  $5.8 \times 10^{10} < Ra < 9.6 \times 10^{11}$ . So far, our measurements at least partially match the physical picture described by Belkadi *et al.* [32] and Liot *et al.* [22]. Especially at the lower end of the Rayleigh number domain, we could not validate that the fluid in the valleys is at rest. Further measurements, particularly measurements of the velocity field, seem to be necessary to clarify this.

Now, we will turn back to the temperature field above the top of the cuboids. In Figs. 3 and 4, we have shown that the mean temperature profile at the rough surface starts to deviate from that at a smooth one if the boundary layer thickness  $\delta_{th}$  falls below the height of the cuboids. However, we could not validate a transition to a fully turbulent boundary layer with an at least partially logarithmic temperature profile (cf. Fig. 5 at the highest Rayleigh number we can set). A view on the distribution of the temperature fluctuations provides some new insights into what happens in this case. To this aim, we plot the probability density function (PDF) of the normalized temperature fluctuations  $\Theta'$  in Fig. 9. To exclude the variation of the boundary layer thickness, which decreases with increasing Rayleigh number and aspect ratio, we have always chosen the position of the maximum of the temperature fluctuations  $z = \delta_{\Theta'}$  for our analysis [cf. Fig. 7(a)]. It is usually located near the outer edge of the (Nusselt-based) boundary layer, but not yet in the bulk region. Castaing *et al.* introduced this as the “mixing zone” [2]. Again, for those cases in which the thermal boundary layer is larger than the roughness height, the PDFs at the rough and the smooth surface (solid and dashed lines, respectively) at a single Rayleigh number collapse quite well. They are clearly skewed towards the temperature at the plate surface  $\Theta = 1$ , showing that the formation of hot thermal plumes dominates the flow in this zone. With increasing Rayleigh number and for those cases in which the boundary layer thickness becomes smaller than the roughness height, the temperature fluctuations  $\Theta'$  become more and more symmetric. This does not happen at the smooth surface. It is interesting to see that this effect appears in the higher Rayleigh number domain,  $5.8 \times 10^{10} < Ra < 9.6 \times 10^{11}$ , as well as in the lower one,  $5.4 \times 10^9 < Ra < 5.9 \times 10^{10}$ , even though the effect is less prominent at lower Rayleigh numbers.

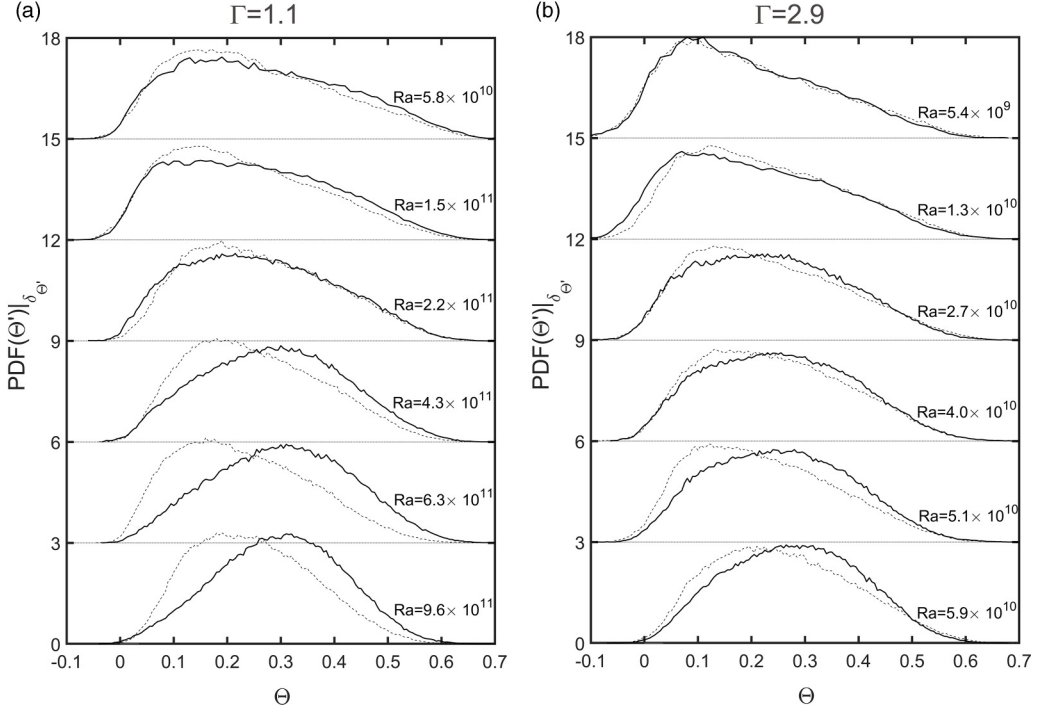


FIG. 9. Probability density function (PDF) of the normalized temperature fluctuations  $\Theta'$  above the top of the cuboids (solid line) compared with PDFs above a smooth surface (dashed line). The PDFs represent the distribution of the fluctuations at the position  $z = \delta_{\Theta'}$  where they exhibit their maximum [cf. Fig. 7(a)]. (a) Data obtained in Configuration I ( $\Gamma = 1.13$ ); (b) data obtained in Configuration II ( $\Gamma = 2.86$ ). The curves are shifted by +3 starting with the highest Rayleigh number at the bottom.

The time-resolved temperature data also enable us to evaluate the distribution of the fluctuations with respect to a potential transition towards turbulence. To this aim, we plot again the PDF of the normalized temperature fluctuations  $\Theta'$  above the top of the cuboids at the position  $z = \delta_{\Theta'}$  in Fig. 10. The data shown are from the measurement at the highest Rayleigh number  $Ra = 9.6 \times 10^{11}$  where a transition is most probable. The distribution of the temperature fluctuations at the edge of the boundary layer is still very close to a Gaussian one. It does not show intermittency indicating a transition towards turbulence [42]. An intermittent distribution of a fluctuating quantity can also be detected computing its kurtosis  $k(\Theta)$ :

$$k(\Theta) = \frac{1}{N} \sum_{i=1}^N \left( \frac{(\Theta_i - \bar{\Theta})}{\Theta'} \right)^4. \quad (12)$$

We use this quantity to analyze the temperature fluctuations at all  $z$ -positions, and we plot the profile  $k(\Theta(z))$  at  $\Gamma = 1.1$  and  $Ra = 9.6 \times 10^{11}$  in Fig. 10(b). If the fluctuations are randomly distributed, the kurtosis amounts to  $k(\Theta) = 3$ . Do they follow an intermittent distribution due to an underlying turbulent flow, their kurtosis is  $k(\Theta) > 3$ . In the figure, we also indicate the position  $z/H = \delta_{\Theta'}/H$ , the distance from the top of the cuboids, where the fluctuations exhibit their maximum, with a dashed-dotted line. For  $z/H < \delta_{\Theta'}/H$ , the flow region that is usually considered as a boundary layer, the kurtosis  $k(\Theta)$  remains close to 3, indicating that the flow is not turbulent there. Only beyond this position does  $k(\Theta)$  start to rise, and it achieves a value of  $k(\Theta) \approx 6$  at  $z/H = 0.025$ . This is true above the rough as well as above the smooth surface, although the rise of  $k(\Theta)$  starts earlier and is steeper at the smooth one. In summary, we have to state here that the temperature field



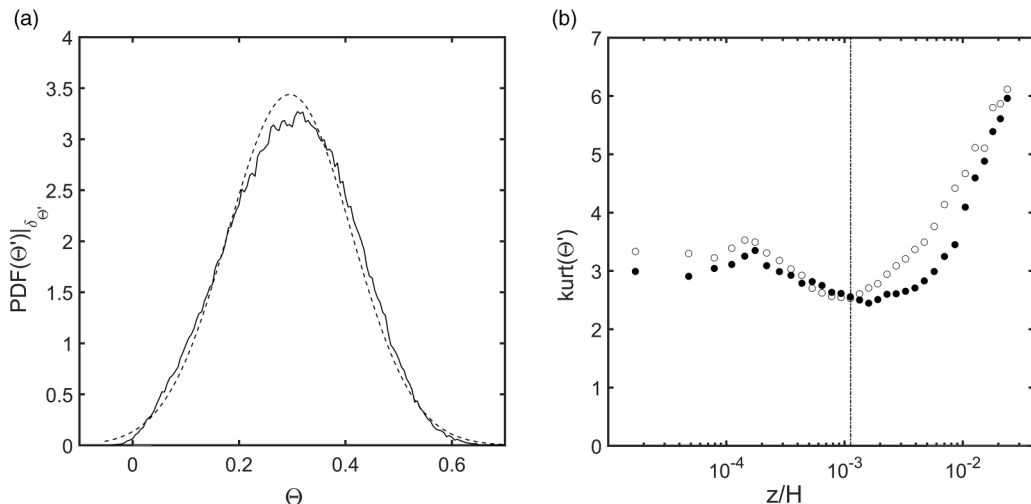


FIG. 10. (a) Probability density function (PDF) of the normalized temperature fluctuations  $\Theta'$  above the top of the cuboids (solid line). The PDF represents the distribution of the fluctuations at the position  $z/H = \delta_{\Theta'}/H$ . The dashed line stands for a Gaussian fit with  $\bar{\Theta} = 0.2952$  and  $\text{var}(\Theta) = 0.01346$ . (b) Profiles of the kurtosis of the temperature fluctuations above the top of the cuboids ( $\bullet$ ) and above a smooth surface ( $\circ$ ). The vertical dashed line indicates the position of the maximum of the temperature fluctuations  $\delta_{\Theta'}$ . All data are obtained at  $\Gamma = 1.1$  and the highest Rayleigh number  $\text{Ra} = 9.6 \times 10^{11}$ .

in the boundary layer above the rough surface does not exhibit any indication of becoming turbulent in the parameter range investigated here. This is indeed in contrast to the velocity measurements reported by Liot *et al.* [22] or the measurements of the global heat flux reported by Russaou en *et al.* [37]. Further measurements, preferably direct velocity measurements, are required to understand this discrepancy.

## V. CONCLUSION

Highly resolved measurements of the near-wall temperature field have been undertaken in turbulent Rayleigh-B enard convection with rough and smooth surfaces. The main aim of our work was to evaluate findings from water experiments and DNSs and whether or not they can be transferred to a low Prandtl number fluid like air. As a second goal, we intended to provide a one-to-one comparison of the near-wall temperature field above a rough and a smooth surface. The experiments have been undertaken in the ‘‘Barrel-of-Ilmenau,’’ a large-scale Rayleigh-B enard experiment. They covered 15 Rayleigh numbers  $5.4 \times 10^9 < \text{Ra} < 9.6 \times 10^{11}$  and two aspect ratios  $\Gamma = 1.1$  and 2.9. We used micro-thermistors of typically 150  $\mu\text{m}$  diameter and 350  $\mu\text{m}$  length to measure profiles of the temperature  $\Theta(z/H)$  and its fluctuations  $\Theta'(z/H)$  above either the rough or the smooth heating plate.

First of all, we could demonstrate that, in analogy to the observation in high Prandtl number fluids, the ratio between the thickness of the thermal boundary layer  $\delta_{\text{th}} = H/(2\text{Nu})$  and the roughness height  $h$  plays a crucial role for the near-wall temperature field, and thus for the convective heat transport at a rough surface. If  $\delta_{\text{th}} > h$ , the temperature field (mean and fluctuations) close to the rough surface do not differ from that at a smooth one. Hence, for those cases the rough surface can be considered as smooth in a good approximation. If  $\delta_{\text{th}}$  becomes smaller than  $h$ , the temperature field above the rough surface starts to differ from that above the smooth one. The mean temperature decreases more slowly towards the bulk, and the distribution of the temperature fluctuations changes from a skewed to an almost symmetrical one. However, we did not find any indication of a transition

of the flow field in the boundary layer to a fully turbulent state. We also show that the temperature always fluctuates in the valleys even at the lowest Rayleigh number  $Ra = 5.4 \times 10^9$  that we have set. However, with increasing  $Ra$ , and if  $\delta_{th}$  becomes smaller than the roughness height  $h$ , the temperature fluctuations increase as well, indicating a stronger motion of the fluid in the valleys. Measurements of the velocity field are necessary to clarify this discrepancy with respect to former measurements by Liot *et al.* [22]. It is also interesting to note that all transitional variations of the temperature field are coupled to the downfall of the Nusselt-based boundary layer thickness below the roughness height, and that this does not depend on the Rayleigh number. Unfortunately, we are not able to set even lower or higher  $Ra$  numbers in our experiment than investigated here. But it might be practicable to close this gap by means of direct numerical simulations.

#### ACKNOWLEDGMENTS

The authors wish to acknowledge the funding by the Deutsche Forschungsgemeinschaft (DFG, German Research Foundation) under Grant No. 495678007. Moreover, they wish to acknowledge Sabine Scherge for her technical assistance running the experiments.

- 
- [1] T. Y. Chu and R. J. Goldstein, Turbulent convection in a horizontal layer of water, *J. Fluid Mech.* **60**, 141 (1973).
  - [2] B. Castaing, G. Gunaratne, F. Heslot, L. Kadanoff, A. Libchaber, S. Thomae, X.-Z. Wu, S. Zaleski, and G. P. Zanetti, Scaling of hard thermal turbulence in Rayleigh-Bénard convection, *J. Fluid Mech.* **204**, 1 (1989).
  - [3] Y.-B. Xin, K.-Q. Xia, and P. Tong, Measured velocity boundary layers in turbulent convection, *Phys. Rev. Lett.* **77**, 1266 (1996).
  - [4] G. Ahlers and X. Xu, Prandtl-number dependence of heat transport in turbulent Rayleigh-Bénard convection, *Phys. Rev. Lett.* **86**, 3320 (2001).
  - [5] J. J. Niemela and K. R. Sreenivasan, Confined turbulent convection, *J. Fluid Mech.* **481**, 355 (2003).
  - [6] O. Shishkina and C. Wagner, Analysis of thermal dissipation rates in turbulent Rayleigh-Bénard convection, *J. Fluid Mech.* **546**, 51 (2006).
  - [7] M. van Reeuwijk, H. J. J. Jonker, and K. Hanjalic, Wind and boundary layers in Rayleigh-Bénard convection. I. Analysis and modeling, *Phys. Rev. E* **77**, 036311 (2008).
  - [8] R. J. A. M. Stevens, R. Verzicco, and D. Lohse, Radial boundary layer structure and Nusselt number in Rayleigh-Bénard convection, *J. Fluid Mech.* **643**, 495 (2010).
  - [9] J. D. Scheel and J. Schumacher, Local boundary layer scales in turbulent Rayleigh-Bénard convection, *J. Fluid Mech.* **758**, 344 (2014).
  - [10] B. I. Shraiman and E. D. Siggia, Heat transport in high-Rayleigh-number convection, *Phys. Rev. A* **42**, 3650 (1990).
  - [11] G. Ahlers, S. Grossmann, and D. Lohse, Heat transfer and large scale dynamics in turbulent Rayleigh-Bénard convection, *Rev. Mod. Phys.* **81**, 503 (2009).
  - [12] D. Lohse and K.-Q. Xia, Small-scale properties of turbulent Rayleigh-Bénard convection, *Annu. Rev. Fluid Mech.* **42**, 335 (2010).
  - [13] F. Chilla and J. Schumacher, New perspectives in turbulent Rayleigh-Bénard convection, *Eur. Phys. J. E* **35**, 58 (2012).
  - [14] Y. Shen, P. Tong, and K.-Q. Xia, Turbulent convection over rough surfaces, *Phys. Rev. Lett.* **76**, 908 (1996).
  - [15] R. H. Kraichnan, Turbulent thermal convection at arbitrary prandtl number, *Phys. Fluids* **5**, 1374 (1962).
  - [16] P.-E. Roche, B. Castaing, B. Chabaud, and B. Hébral, Observation of the 1/2 power law in Rayleigh-Bénard convection, *Phys. Rev. E* **63**, 045303(R) (2001).

- [17] Y.-B. Du and P. Tong, Enhanced heat transport in turbulent convection over a rough surface, *Phys. Rev. Lett.* **81**, 987 (1998).
- [18] P. Wei, T.-S. Chan, R. Ni, X.-Z. Zhao, and K.-Q. Xia, Heat transport properties of plates with smooth and rough surfaces in turbulent thermal convection, *J. Fluid Mech.* **740**, 28 (2014).
- [19] Y.-C. Xie and K.-Q. Xia, Turbulent thermal convection over rough plates with varying roughness geometries, *J. Fluid Mech.* **825**, 573 (2017).
- [20] S. Ciliberto and C. Laroche, Random roughness of boundary increases the turbulent convection scaling exponent, *Phys. Rev. Lett.* **82**, 3998 (1999).
- [21] J.-C. Tisserand, M. Creyssels, Y. Gasteuil, H. Pabiou, M. Gibert, B. Castaing, and F. Chilla, Comparison between rough and smooth plates within the same Rayleigh-Bénard cell, *Phys. Fluids* **23**, 015105 (2011).
- [22] O. Liot, J. Salort, R. Kaiser, R. du Puits, and F. Chillà, Boundary layer structure in a rough Rayleigh-Bénard cell filled with air, *J. Fluid Mech.* **786**, 275 (2016).
- [23] M. J. Tummers and M. Steunebrink, Effect of surface roughness on heat transfer in Rayleigh-Bénard convection, *Int. J. Heat Mass Transf.* **139**, 1056 (2019).
- [24] M. Belkadi, L. Guislain, A. Sergent, B. Podvin, F. Chillà, and J. Salort, Experimental and numerical shadowgraph in turbulent Rayleigh-Bénard convection with a rough boundary: Investigation of plumes, *J. Fluid Mech.* **895**, A7 (2020).
- [25] H. Jiang, X. Zhu, V. Mathai, R. Verzicco, D. Lohse, and C. Sun, Controlling heat transport and flow structures in thermal turbulence using ratchet surfaces, *Phys. Rev. Lett.* **120**, 044501 (2018).
- [26] S. Toppaladoddi, S. Succi, and J. S. Wettlaufer, Roughness as a route to the ultimate regime of thermal convection, *Phys. Rev. Lett.* **118**, 074503 (2017).
- [27] X. Zhu, R. J. A. M. Stevens, R. Verzicco, and D. Lohse, Roughness-facilitated local 1/2 scaling does not imply the onset of the ultimate regime of thermal convection, *Phys. Rev. Lett.* **119**, 154501 (2017).
- [28] K. Chand, A. K. De, and P. K. Mishra, Enhanced heat flux and flow structures in turbulent Rayleigh-Bénard convection with rough boundaries, *Phys. Rev. Fluids* **6**, 124605 (2021).
- [29] P. K. Kar, U. Chetan, J. Mahato, T. L. Sahu, P. K. Das, and R. Lakkaraju, Heat flux enhancement by regular surface protrusion in partitioned thermal convection, *Phys. Fluids* **34**, 127105 (2022).
- [30] O. Shishkina and C. Wagner, Modelling the influence of wall roughness on heat transfer in thermal convection, *J. Fluid Mech.* **686**, 568 (2011).
- [31] Y.-Z. Zhang, C. Sun, Y. Bao, and Q. Zhou, How surface roughness reduces heat transport for small roughness heights in turbulent Rayleigh-Bénard convection, *J. Fluid Mech.* **836**, R2 (2018).
- [32] M. Belkadi, A. Sergent, Y. Fraigneau, and B. Podvin, On the role of roughness valleys in turbulent Rayleigh-Bénard convection, *J. Fluid Mech.* **923**, A6 (2021).
- [33] H. Jiang, D. Wang, Y. Cheng, H. Hao, and C. Sun, Effects of ratchet surfaces on inclined thermal convection, *Phys. Fluids* **35**, 015130 (2023).
- [34] S. Wagner and O. Shishkina, Heat flux enhancement by regular surface roughness in turbulent thermal convection, *J. Fluid Mech.* **763**, 109 (2015).
- [35] E. Villiermaux, Transfer at rough sheared interfaces, *Phys. Rev. Lett.* **81**, 4859 (1998).
- [36] X. Zhu, R. J. A. M. Stevens, O. Shishkina, R. Verzicco, and D. Lohse,  $Nu \sim Ra^{1/2}$  scaling enabled by multiscale wall roughness in Rayleigh-Bénard turbulence, *J. Fluid Mech.* **869**, R4 (2019).
- [37] E. Rusaouën, O. Liot, B. Castaing, J. Salort, and F. Chillà, Thermal transfer in Rayleigh-Bénard cell with smooth or rough boundaries, *J. Fluid Mech.* **837**, 443 (2018).
- [38] R. du Puits, C. Resagk, and A. Thess, Thermal boundary layers in turbulent Rayleigh-Bénard convection at aspect ratios between 1 and 9, *New J. Phys.* **15**, 013040 (2013).
- [39] J. Salort, O. Liot, E. Rusaouen, F. Seychelles, J.-C. Tisserand, M. Creyssels, B. Castaing, and F. Chillà, Thermal boundary layer near roughnesses in turbulent Rayleigh Bénard convection: Flow structure and multistability, *Phys. Fluids* **26**, 015112 (2014).
- [40] R. J. A. M. Stevens, E. P. van der Poel, S. Grossmann, and D. Lohse, The unifying theory of scaling in thermal convection: The updated prefactors, *J. Fluid Mech.* **730**, 295 (2013).
- [41] H. Schlichting and K. Gersten, *Boundary Layer Theory* (Springer-Verlag, Berlin, 2016).
- [42] D. Lohse and S. Grossmann, Intermittency in turbulence, *Physica A* **194**, 519 (1993).